

Diffusion behavior of hydrogen isotopes in tungsten revisited by molecular dynamics simulations

Mingjie Qiu(丘明杰), Lei Zhai(翟磊), Jiechao Cui(崔节超), Baoqin Fu(付宝勤), Min Li(李敏), Qing Hou(侯氢)
Citation: Chin. Phys. B . 2018, 27(7): 073103. **doi:** 10.1088/1674-1056/27/7/073103

Journal homepage: http://cpb.iphy.ac.cn; http://iopscience.iop.org/cpb

What follows is a list of articles you may be interested in

Anisotropic self-diffusion of fluorinated poly(methacrylate) in metal-organic frameworks assessed with molecular dynamics simulation

Tao Lu(鲁桃), Biao Xu(徐彪), Fei-Hong Ye(叶飞宏), Xin-Hui Zhou(周馨慧), Yun-Qing Lu(陆云清), Jin Wang(王瑾)
Chin. Phys. B . 2017, 26(12): 123104. **doi:** 10.1088/1674-1056/26/12/123104

First-principles study of solute diffusion in Ni_3Al

Shaohua Liu(刘少华), Zi Li(李孜), Chongyu Wang(王崇愚)
Chin. Phys. B . 2017, 26(9): 093102. **doi:** 10.1088/1674-1056/26/9/093102

Effect of grain boundary structures on the behavior of He defects in Ni: An atomistic study

H F Gong(龚恒风), Y Yan(严岩), X S Zhang(张显生), W Lv(吕伟), T Liu(刘彤), Q S Ren(任啟森)
Chin. Phys. B . 2017, 26(9): 093104. **doi:** 10.1088/1674-1056/26/9/093104

Wetting and coalescence of the liquid metal on the metal substrate

Zhen-Yang Zhao(赵珍阳), Tao Li(李涛), Yun-Rui Duan(段云瑞), Zhi-Chao Wang(王志超), Hui Li(李辉)
Chin. Phys. B . 2017, 26(8): 083104. **doi:** 0.1088/1674-1056/26/8/083104

Molecular dynamics simulation of decomposition and thermal conductivity of methane hydrate in porous media

Ping Guo(郭平), Yi-Kun Pan(潘意坤), Long-Long Li(李龙龙), Bin Tang(唐斌)
Chin. Phys. B . 2017, 26(7): 073101. **doi:** 10.1088/1674-1056/26/7/073101

Diffusion behavior of hydrogen isotopes in tungsten revisited by molecular dynamics simulations*

Mingjie Qiu(丘明杰), Lei Zhai(翟磊), Jiechao Cui(崔节超),
Baoqin Fu(付宝勤), Min Li(李敏), and Qing Hou(侯氢)†

Key Laboratory for Radiation Physics and Technology (Ministry of Education), Institute of Nuclear Science and Technology, Sichuan University, Chengdu 610064, *China*

(Received 10 January 2018; revised manuscript received 26 April 2018; published online 25 June 2018)

Molecular dynamics simulations were performed to study the diffusion behavior of hydrogen isotopes in single-crystal tungsten in the temperature range of 300–2000 K. The simulations show that the diffusion coefficient of H isotopes exhibits non-Arrhenius behavior, though this deviation from Arrhenius behavior is slight. Many-body and anharmonic effects of the potential surface may induce slight isotope-dependence by the activation energy; however, the dependence of the pre-factor of the diffusion coefficient on the isotope mass is diminished. The simulation results for H-atom migration near W surfaces suggest that no trap mutations occur for H atoms diffusing near either W{100} or W{111} surfaces, in contrast to the findings for He diffusion near W surfaces. Based on the H behavior obtained by our MD simulations, the time evolution of the concentration distribution of interstitial H atoms in a semi-infinite W single crystal irradiated by energetic H projectiles was calculated. The effect of H concentration on H diffusion is discussed, and the applicability of the diffusion coefficients obtained for dilute H in W is assessed.

Keywords: hydrogen isotopes, tungsten, diffusion, molecular dynamics

PACS: 31.15.xv, 52.40.Hf, 52.65.Yy, 66.30.J– **DOI:** 10.1088/1674-1056/27/7/073103

1. Introduction

As a plasma-facing material in nuclear fusion reactors, tungsten suffers bombardment by high-flux hydrogen and helium isotopes (H, D, T, He) in the fusion environment.[1–3] The implantation of large numbers of hydrogen and helium isotopes into the W lining could induce changes in its structural and thermomechanical properties. Moreover, high-dose radioactive T, which is a fusion fuel, could pose a crucial safety issue in the event of lining failure.[4] Thus, the retention of hydrogen isotopes in W is an important research subject that has attracted intensive experimental and theoretical attention, as reviewed in Refs. [5]–[8].

Nuclear reaction analysis (NRA), which detects the concentration profile of H in bulk W,[9] and thermal desorption spectroscopy (TDS),[10,11] which measures the rate of H released from W, are two major experimental techniques used to study the mechanism of H retention in W (we shall use the chemical symbol H to refer to any hydrogen isotope, if not otherwise specified). To analyze and extract the underlying H-retention mechanism, rate-equation-based modelling of the experimental observations can be performed.[10–12] The models for diffusion, trapping, surface effects, and so on adopted in this rate-equation-based modelling significantly impact the explanation of experimental observations.[10,11,13–17] However, rate-equation-based modelling itself is phenomenological. The establishment of the models requires a detailed understanding of the relevant atomistic processes, in which atomistic simulation plays an indispensable role.[18] The purpose of the present work is to study the diffusion behavior of interstitial H atoms in the bulk and near-surface of W, which is a basic atomistic process involved in the time evolution of H retention in W.

The diffusion behavior of interstitial H atoms in bulk W has been studied by a number of authors using density functional theory (DFT).[19–23] All the DFT calculations concluded that the tetrahedral sites in single-crystal W are the most preferable for occupation by interstitial H atoms. This conclusion is consistent with experimental observations.[24] However, the calculated activation energies for the diffusion of H between two adjacent tetrahedral sites can vary widely: 0.20 eV,[19,23] 0.21 eV,[22] 0.332 eV,[20] and 0.38 eV.[21] Among these results, the last activation energy, obtained by Johnson *et al.*,[21] best agrees with that experimentally obtained by Frauenfelder,[12] which is considered to be the most reliable experimental result to date.[5] Nevertheless, it should be noted that Frauenfelder conducted his measurements of the diffusion coefficient of D in W at high temperature (> 1100 K) and deduced the activation energy according to the Arrhenius relationship. Several recent studies on the diffusion of He in W have shown that the diffusion behavior of interstitial He tends to be non-Arrhenius at high temperature (> 650 K).[25–27] These results for He diffusion in W suggest that it would be worthwhile to examine whether the diffusion of H in W also tends to be non-Arrhenius at high temperature. Because

*Project supported by the National Magnetic Confinement Fusion Program of China (Grant No. 2013GB109002).
†Corresponding author. E-mail: qhou@scu.edu.cn
© 2018 Chinese Physical Society and IOP Publishing Ltd

the DFT method is applicable to calculating the static energy states of atomic systems and the temperature-dependence of the diffusion coefficient for H in W presuming Arrhenius behavior, this examination can be performed only by using the molecular dynamics (MD) approach. Another issue worthy of investigation is the isotopic effect of H diffusion. The isotopic effect is usually considered in terms of the harmonic transition state theory (HTST). If the thermal vibrations of H isotopes dominantly contribute to the pre-factor of the diffusion coefficient, the pre-factor would be inversely proportional to the square root of the atomic mass. However, with increasing temperature, the anharmonic properties of the potential surface and nonlinear multiphononic contributions could exert effects.

Recent studies on the diffusion behavior of He near W surfaces[28–30] inspired us to consider the analogous diffusion behavior of H atoms. MD simulations have shown that He atoms near W{100} and {110} surfaces can quickly escape from the substrate, while trap mutations most likely occur when the He atoms migrate to the W{111} surface. The trap mutations may impede the release of He atoms from the substrate and would impact the analysis in TDS experiments. Thus, whether trap mutations occur in the case of H-atom migration near W surfaces also merits further investigation.

In the present paper, MD simulations were conducted to study the diffusion behavior of H in W. The surface and isotopic effects, as well as the impact of H concentration, on H diffusion will be discussed. A general description of this method is presented in Section 2, followed by the results in Section 3. Finally, the findings are discussed and concluding remarks are given in Section 4.

2. Simulation method

2.1. MD simulation

Our MD simulations were performed using the graphics processing unit (GPU)-based MD package MDPSCU.[31] For the inter-atomic potentials, we implemented the embedded-atom-method (EAM) potentials developed by Bonny *et al.*[32] for the W–H–He system on the basis of the W–W potential of Marinica *et al.*[33] Only the potential denoted as EAM1 in Ref. [32] was used. All the simulations were performed in the temperature range of 300–2000 K. For W, the lattice constant $a_0 = 3.14$ Å was adopted, which is consistent with that used by Marinica *et al.*[33]

In calculating the H diffusion coefficient, 1000 independent simulation boxes were generated for body-centered-cubic (bcc) W. Each box has a size of $10a_0 \times 10a_0 \times 10a_0$ and contains 2000 W atoms. Periodic boundary conditions were applied in the x-, y-, and z-directions. In the simulation procedure, we initially added one H atom to every simulation box, and then thermalized them to a given temperature by the Monte Carlo sampling of the Maxwell distribution for the velocities of the atoms. After achieving thermal equilibrium, the boxes were then allowed to freely relax for 40 ps with the integral time step of 0.25 fs. The time step is small enough to guarantee the energy conservation. Since the energies of the boxes follow the Boltzmann distribution at the given temperature, an NVT ensemble is simulated. The displacement $R(t)$ of the H atom was recorded. The diffusion coefficient D at a given temperature was then calculated by linear fitting the equation

$$\langle R^2(t)\rangle = 6Dt, \tag{1}$$

where t is the time and $\langle R^2(t)\rangle$ denotes the ensemble average.

To study the diffusion behavior of H atoms near surfaces, we constructed W{100} and W{111} surfaces with bcc W box sizes of $10a_0 \times 10a_0 \times 30a_0$ and $8.5a_0 \times 9.8a_0 \times 27.7a_0$, respectively. Generally, the simulation procedure consisted of two phases. In the first phase, one H atom was randomly introduced into the constructed bcc W box, and periodic boundary conditions were used in all directions. For each of the box sizes, we generated 500 independent replicas that were subsequently thermalized to a given temperature. In the second phase, the periodic boundary condition in the z-direction was discarded, which is defined as the (100) and (111) crystal orientations. The length of the box side in the z-direction was sufficient to eliminate possible interactions between the two surfaces. In this phase, all the boxes were evolved for 1000 ps, during which the states of the boxes were recorded every 20 ps.

3. Simulation results

3.1. Non-Arrhenius diffusion of H in W

Using the methods described above, the diffusion coefficients D of H, D, and T in W were calculated in the temperature range of 300–2000 K and fitted to the Arrhenius relationship

$$D = D_0 \exp\left(-\frac{E_a}{k_B T}\right), \tag{2}$$

as shown in Fig. 1. Here, D_0 is the pre-exponential factor (or pre-factor), E_a is the activation energy, k_B is the Boltzmann constant, and T is the temperature (K). At first sight, the dependence of D on temperature follows the Arrhenius relationship well, with the corresponding D_0 and E_a values for H, D, and T presented in Table 1. However, detailed analysis shows that E_a varies with the temperature range chosen when fitting the MD data to Eq. (2). For example, over the whole temperature range, fitting the MD data for an H atom to Eq. (2) results in $E_a = 0.218 \pm 0.002$ eV (Table 1), while the E_a values obtained in the discrete temperature ranges of 300–1000 K, 1000–2000 K, and 1600–2000 K are 0.221 ± 0.002 eV, 0.201 ± 0.004 eV, and 0.183 ± 0.003 eV,

respectively. In the low-temperature range (300–1000 K), the E_a value (0.221 eV) is in good agreement with the diffusion barrier of 0.221 eV that we obtained using the nudged elastic band (NEB) method.[34,35] This can be understood because the NEB is a static method which calculates the lowest diffusion barrier on the potential surface at 0 K. However, with increasing temperature, E_a decreases, and could even be smaller than the diffusion barrier of the NEB. This variation of E_a is an indication of non-Arrhenius diffusion. A similar phenomenon has been observed for He in W by Wang *et al.*,[25] Shu *et al.*,[36] Perez *et al.*,[27] and Wen *et al.*[37] The E_a value of He atoms in W is lower in the temperature range 650–1000 K than that at 300–650 K.[25,27,37] At temperatures higher than 1000 K, the diffusion of He atoms in W tends to be the Einstein–Smoluchowski type,[37] which would result in an enlarged E_a if arbitrarily fitted to the Arrhenius relationship. The mechanism of multiple diffusion pathways, proposed by Wang *et al.*[25] and Shu *etal.*,[36] cannot explain the lowered E_a in the intermediate temperature range (650–1000 K). The reason is as follows. According to HTST for multiple diffusion pathways, the diffusion coefficient D can be expressed as

$$\begin{aligned} D &= \sum_{i=0}^{m} D_i \mathrm{e}^{-\frac{E_i}{k_\mathrm{B}T}} \\ &= D_0 \mathrm{e}^{-\frac{E_0}{k_\mathrm{B}T}} \left(1 + \sum_{i=1}^{m} \frac{D_i}{D_0} \mathrm{e}^{-\frac{E_i - E_0}{k_\mathrm{B}T}}\right), \end{aligned} \tag{3}$$

where D_i and E_i represent the pre-factor and activation energy of diffusion pathway i. E_0 is the lowest activation energy. The logarithm of diffusivity $\ln D$ can be expressed as

$$\ln D = -\frac{E_0}{k_\mathrm{B}T} + \ln D_0 + \ln\left(1 + \sum_{i=1}^{m} \frac{D_i}{D_0} \mathrm{e}^{-\frac{E_i - E_0}{k_\mathrm{B}T}}\right). \tag{4}$$

Because $E_0 < E_i$, $\ln D$ tends to be $-\frac{E_0}{k_\mathrm{B}T} + \ln D_0$ and $\frac{\partial \ln D}{\partial(1/T)} = -E_0/k_\mathrm{B}$ at the limit $T \to 0$. It is easy to prove that $\frac{\partial \ln D}{\partial(1/T)}$ is always less than $-E_0/k_\mathrm{B}$ and monotonically decreases with increasing temperature T. In other words, the activation energy obtained by fitting the Arrhenius relationship would increase with increasing temperature. Wen and coworkers suggested that the deviation from HTST prediction could be the result of many-body effects.[37] Alternatively, we conjecture that the existence of correlated successive jumps, which have been observed in the diffusion of metallic adatoms on surfaces,[38] is a more likely explanation for the non-Arrhenius diffusion of He and H isotopes in W. In comparison with the non-Arrhenius diffusion of He in W, the non-Arrhenius behavior for H in W is insignificant, because the lowest diffusion barrier for H in W is higher than the lowest diffusion barrier for He in W. Non-Arrhenius diffusion for H in W tends to occur at a higher temperature than for He in W, and the transition to Einstein–Smoluchowski diffusion is not observed up to the highest temperature (2000 K) considered in the present paper. The non-Arrhenius diffusion of H in W has been more obviously observed in the MD simulations of Liu *et al.*,[39] who used a different potential for the H–W system than ours. However, in contrast to our findings, they observed E_a increasing as temperature increased, and an E_a in the low temperature region that was less than the value they obtained by NEB using their potential.

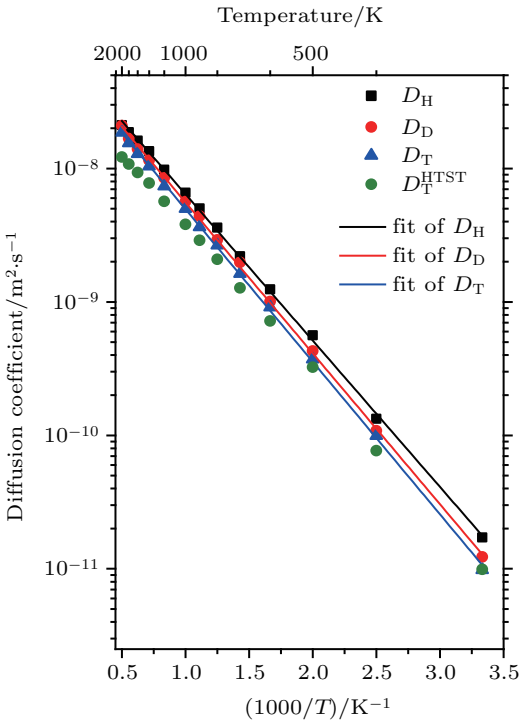


Fig. 1. (color online) Diffusion coefficients of H, D, and T in W, calculated by MD simulation (D_H, D_D, and D_T), by fitting the Arrhenius relationship to the MD data (lines). $D_\mathrm{T}^\mathrm{HTST}$ is the diffusion coefficient of T, derived from D_H based on single-mode harmonic transition state theory.

Table 1. Fitted pre-exponential factors and activation energies for H, D, and T and a comparison with literature data.

	H isotopes	D_0/m^2·s^{-1}	E_a/eV	NEB: E_a/eV
Present work	H	$(8.03 \pm 0.012) \times 10^{-8}$	0.218 ± 0.002	0.211
	D	$(7.551 \pm 0.025) \times 10^{-8}$	0.225 ± 0.001	0.211
	T	$(6.902 \pm 0.017) \times 10^{-8}$	0.227 ± 0.001	0.211
Frauenfelder[12] (1100–2500 K)	H	4.1×10^{-7}	0.391	
Frauenfelder[22] (1500–2500 K)	H	1.58×10^{-7}	0.25	
Heinola *et al.*[22]	H	5.2×10^{-8}	0.21	
Johnson *et al.*[21]	H	8.93×10^{-7}	0.38	

For comparison with experimental results, the activation energies obtained by separately fitting the Arrhenius relationship to Frauenfelder's experimental data in the temperature ranges of 1100–2500 K and 1500–2500 K are 0.39 eV and 0.25 eV, respectively.[22] The observation that the E_a at higher temperatures is smaller than that at lower temperatures is similar to our results shown above. However, the effect of non-Arrhenius diffusion on the experimental observations remains ambiguous because of the large discrepancies between E_a values obtained through experiments and simulations.

3.2. Isotopic effects of H diffusion in W

According to the HTST of Vineyard,[40] E_a is independent of isotopic mass, and the pre-factor in Eq. (2) for isotopes can be written as

$$D_{0,\alpha}^{(\mathrm{HTST})} = \frac{A}{\sqrt{\bar{m}_\alpha}}, \tag{5}$$

where α denotes the isotopes (H, T, D), A is a constant, and $\bar{m}_\alpha$ is the effective mass. Vineyard showed that $\bar{m}_\alpha$ is dependent on the masses of the jumping atom (here, H, D, or T) and the host atom (W), as well as the direction of the diffusion path at the saddle point on the potential surface. $\bar{m}_\alpha$ would be well approximated by the mass of the jumping atom if its movement is the dominant contribution to the configuration variation during jumping. By this approximation, the diffusion coefficients for D and T can be expressed by

$$D_{\alpha}^{(\mathrm{HTST})} = \sqrt{\frac{m_\mathrm{H}}{m_\alpha}} D_\mathrm{H}, \tag{6}$$

where D_H is the diffusion coefficient of the H atom. In Fig. 1, the diffusion coefficient $D_\mathrm{T}^{(\mathrm{HTST})}$ is compared to the diffusion coefficient D_T obtained by MD simulation. $D_\mathrm{T}^{(\mathrm{HTST})}$ agrees well with D_T at low temperature but deviates from D_T with increasing temperature. The difference arises from two sources, as discussed below.

First, from Table 1, the pre-factors calculated via the MD simulations give the ratio $D_{0,\mathrm{T}}/D_{0,\mathrm{H}} = 0.93$. This value is larger than $\sqrt{m_\mathrm{H}/m_\mathrm{T}} = 0.58$, the ratio predicted by Eq. (6). From Eq. (5), when the value of $D_{0,\mathrm{T}}/D_{0,\mathrm{H}}$ approaches unity, the effective masses $\bar{m}_\mathrm{H}$ and $\bar{m}_\mathrm{T}$ are similar. According to Vineyard's analysis,[40] the underlying physical mechanism is that many-body effects play roles: the W atoms neighboring the jumping atom (H or T) are displaced non-symmetrically as the jumping atom passes through the saddle point of the potential surface, and thus, the W atoms impart a large contribution to the effective mass. The situation is similar for the diffusion of D, with $D_{0,\mathrm{D}}/D_{0,\mathrm{H}} = 0.97$ vs. $\sqrt{m_\mathrm{H}/m_\mathrm{D}} = 0.71$. Second, also from Table 1, differences exist among the E_a values obtained by MD simulations for H, D, and T. Although the differences are small, they contradict the predictions of the HTST, in which E_a is constant for isotopes. Since MD is based on classical mechanics, the differences among the E_a values of the isotopes do not arise from the contribution of the zero-point energy (ZPE), which is an isotope-dependent quantum effect that was added to E_a in previous studies.[21,22] Moreover, it has been shown that including the ZPE in E_a leads to a more temperature-dependent diffusion-coefficient pre-factor than when the ZPE is not included.[23] Clearly, the dependence of E_a on isotope identity observed in the present paper derives from the anharmonic properties of the potential surface.

3.3. Migration of H atoms near W surfaces

MD simulations were performed for temperatures from 600–1600 K with the simulation boxes having two free surfaces. Two surface orientations, {100} and {111}, were considered.

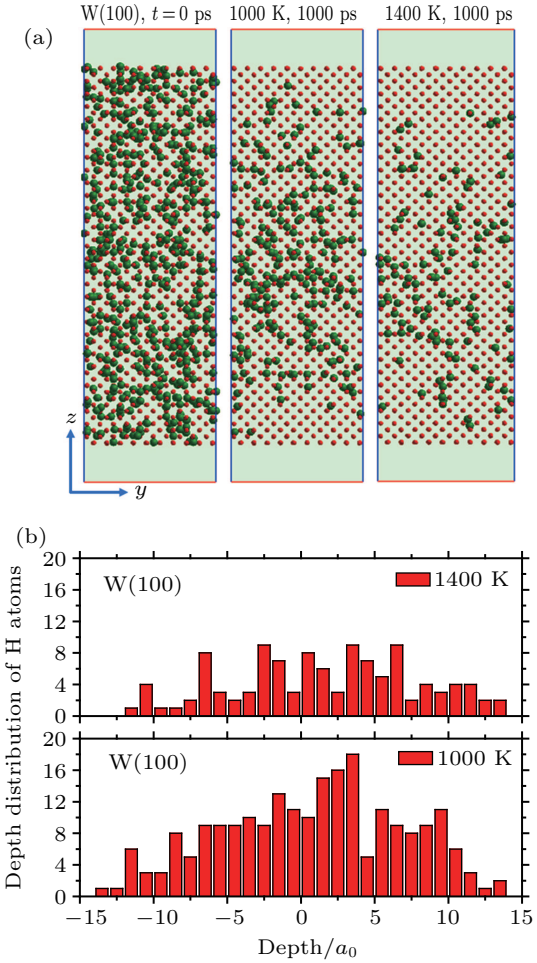


Fig. 2. (color online) (a) Snapshots of H-atom distribution in W bulk for W(100); $t = 0$ and 1000 ps; and $T = 1000$ K and 1400 K. Each picture represents the merging of 500 simulation boxes. The red and green spheres represent W and H atoms, respectively. (b) The corresponding depth distribution of H atoms.

For the case of the W{100} surface, figure 2(a) displays snapshots taken at times $t = 0$ and 1000 ps for temperatures $T = 1000$ K and 1400 K. The snapshots were generated by merging snapshots of 500 simulation boxes. From the figure, the interstitial H atoms are initially uniformly distributed in

the simulation boxes. As time elapses, some of the H atoms escape from the substrate, and dilute H atoms are found in the subsurface region. Figure 2(b) shows the corresponding depth distribution of H atoms. These results suggest that H atoms near the surface can quickly escape from the substrate, analogous to the behavior of He atoms near the W{001} surface.[30] The time scale for the escape of subsurface H atoms should be shorter than the recording interval (20 ps).

Figure 3 displays the snapshots and depth distribution of H atoms for the case of the W{111} surface orientation, which is in the closest-packed direction of W atoms. In the case of He atoms in W, temperature-dependent trap mutations may occur when He atoms move to the W{111} surface, and these trap mutations induce the subsurface accumulation of He atoms.[28,30] We repeated the MD simulation of He diffusion near the W{111} surface using the W–H–He potential of Bonny *et al.*,[32] which is used in the present paper for the W–H interaction but is different from the W–He potentials used in Ref. [28] and [30]. The simulation results (not shown in the present paper) further verify the accumulation of He atoms in the subsurface region of the W{111} surface. However, in contrast to the He case, no subsurface accumulation of H atoms is observed in Fig. 3. Similarly to the case of H diffusion near the W{100} surface described above, H atoms can quickly escape from the substrate through the W{111} surface. This observation is applicable to all temperatures considered in the present paper.

Because the time scale for the escape of subsurface H atoms from the substrate is much smaller than the time scale considered in continuous-diffusion-theory (CDT)-based simulations (e.g., the size of the time grid in rate theory), we can establish a model for continuous diffusion for W surfaces. In this model, the W surface is treated as an absorber. The H atoms can be considered to migrate through the bulk tungsten until arriving at the absorber, where they are absorbed instantly with probability R. According to Wang *et al.*,[30] R can be determined by fitting the MD data and the following formula

$$N_{\mathrm{a}}(t)/N_{\mathrm{B}} = \left[1 - \int_{-h}^{h} \mathrm{d}z \frac{n_0(z)}{2}(E_1 + E_2 + E_3 + E_4)\right], \quad (7)$$

with

$$E_1 = \sum_{k=0}^{\infty} (1-2R)^k \mathrm{erf}\left[\frac{h + (-1)^k (2kh - z)}{\sqrt{4Dt}}\right],$$

$$E_2 = \sum_{k=0}^{\infty} (1-2R)^k \mathrm{erf}\left[\frac{h + (-1)^{k+1} (2kh - z)}{\sqrt{4Dt}}\right],$$

$$E_3 = \sum_{k=1}^{\infty} (1-2R)^k \mathrm{erf}\left[\frac{h + (-1)^{k+1} (2kh + z)}{\sqrt{4Dt}}\right],$$

$$E_4 = \sum_{k=1}^{\infty} (1-2R)^k \mathrm{erf}\left[\frac{h + (-1)^{k} (2kh + z)}{\sqrt{4Dt}}\right],$$

where $N_{\mathrm{a}}(t)$ is the accumulated number of H atoms escaping from the substrate in time t, and N_{B} is the number of simulation boxes, which equals the total H atoms (here, $N_{\mathrm{B}} = 500$). D is the diffusion coefficient of H in the W bulk calculated above. The $n_0(z)$ term represents the initial depth distribution of the H atoms and is given by $1/L_z$ (L_z is the simulation box size in the z-direction) since the H atoms are initially uniformly distributed in the simulation boxes. h is the distance from the center of the simulation box to the absorbing layer, and is defined as $h = L_z/2$ here.

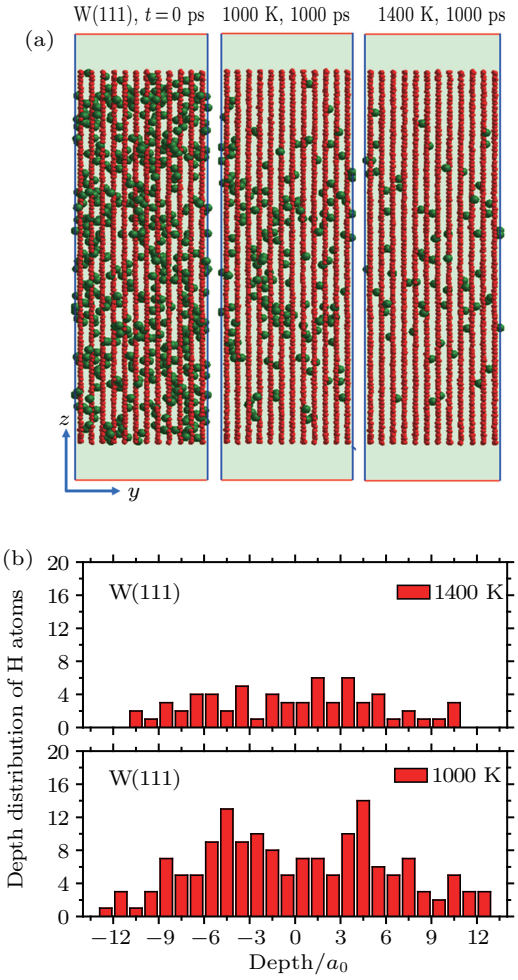


Fig. 3. (color online) (a) Snapshots of H-atom distribution in W bulk for W(111); $t = 0$ and 1000 ps; and $T = 1000$ K and 1400 K. Each picture represents the merging of 500 simulation boxes. The red and green spheres represent W and H atoms, respectively. (b) The corresponding depth distribution of H atoms.

The absorbing probabilities R determined for the W{100} and W{111} surfaces are summarized in Table 2 for different substrate temperatures. Figure 4 shows $N_{\mathrm{a}}(t)/N_{\mathrm{B}}$ obtained by MD simulations as well as by Eq. (7). Generally, the MD results are well described by Eq. (7), suggesting validation of the absorber model. By CDT, the value of R should be 1 for a perfect absorber. As we can see from Table 2, the R value for W{100} is less than 1 while that for W{111} is greater than 1. The deviation of the R value from 1 reveals that the

diffusion barriers of H atoms near the surfaces vary relative to the in-bulk diffusion barriers. Using the NEB method, we calculated the potential evolution for an H atom moving from the near-surface region to the top of the surface. The results are shown in Fig. 5. It should be noted that the horizontal axis represents the configuration images of the NEB rather than the depth of the H atoms in W. Thus, for the W{111} surface, the interstitial state of an H atom close to the surface has a potential energy lower than that of the in-bulk interstitial state by 0.07 eV, while for the W{100} surface, the interstitial state of a near-surface H atom has almost the same potential energy as the in-bulk interstitial state. This observation explains why the R value is larger than 1 for the W{111} surface and smaller than 1 for the W{100} surface. Meanwhile, the energy difference from the bulk to the surface is approximately 1.50 eV, which is in good agreement with the absorption energy (from the surface to the bulk) calculated by Hodille *et al.*[41]

Table 2. R values obtained by fitting Eq. (10) to simulation data. The diffusion coefficient used in Eq. (10) is calculated in the present work.

Temperature/K	Diffusion coefficient/$m^2 \cdot s^{-1}$	R for W{100}	R for W{111}
600	1.244×10^{-9}	0.809	0.937
800	3.607×10^{-9}	0.944	1.232
1000	6.593×10^{-9}	0.925	1.140
1200	9.796×10^{-9}	0.977	1.086
1400	1.347×10^{-8}	0.938	1.097
1600	1.616×10^{-8}	0.931	1.112

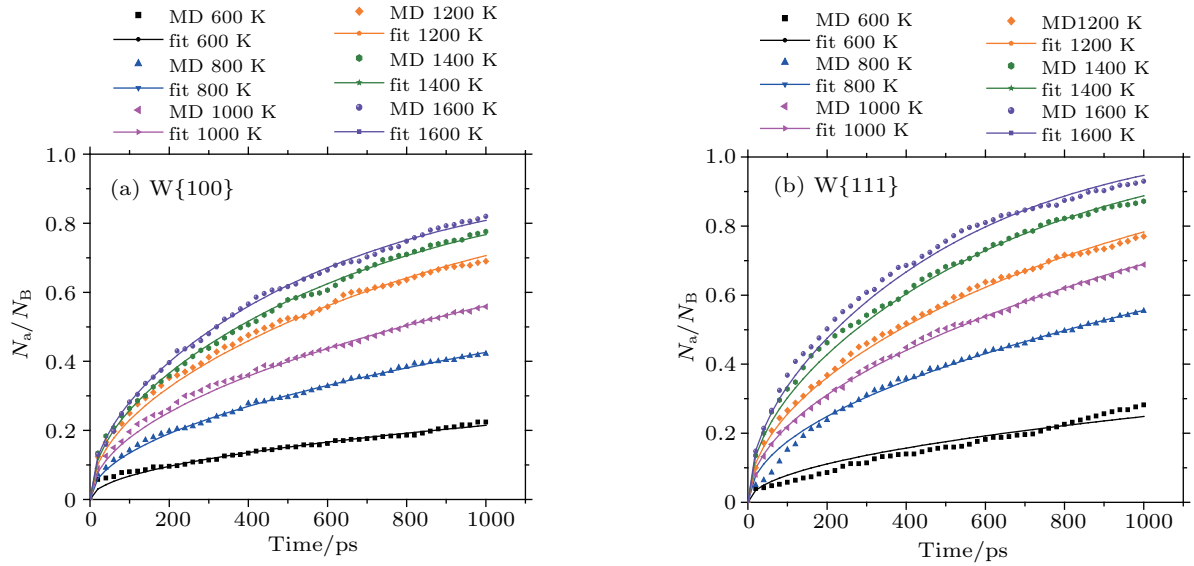


Fig. 4. (color online) The ratio of escaping H atoms (N_a) to the total H atoms (N_B) as a function of time obtained from MD simulations for (a) W{100} and (b) W{111} surfaces. The solid lines are the curves generated from the fitting of Eq. (10) to the MD data.

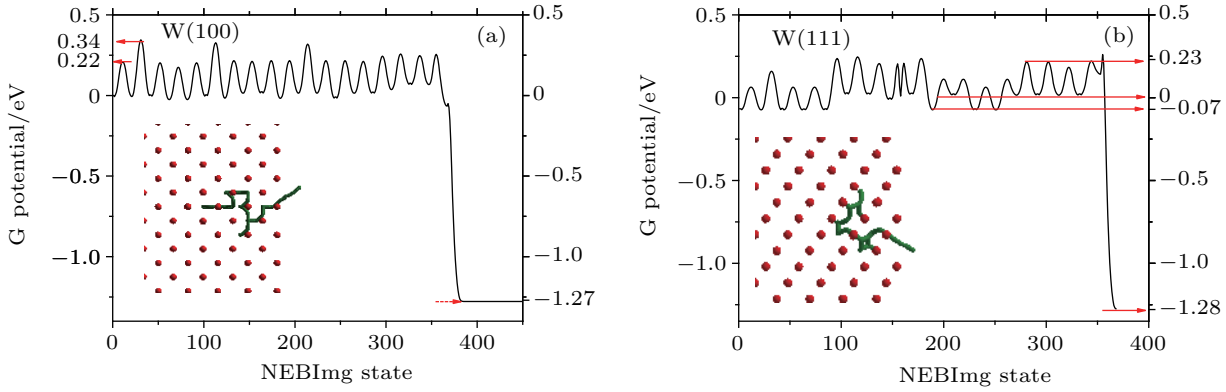


Fig. 5. (color online) Evolution of the potential barrier for H-atom movement in the near-surface region until escaping from the surface: (a) for W{100} and (b) for W{111} surfaces. The potential energy of the in-bulk tetrahedral interstitial state is taken as zero.

We note that the W–H potential used in this paper is repulsive if H atoms are on the top of the W surfaces. No H adatoms, and thus, no H_2 molecules, which are thought to be detected in TDS experiments, are observed on the top of the W surfaces in our MD simulations. The study of the diffusion, recombination, and desorption of H adatoms on W surfaces likely needs a H–W potential that can correctly describe the interaction between H adatoms and W surface atoms. However, the model established here can be applied to modelling the production rate of H adatoms on W surfaces produced by diffusing in-bulk H atoms. The behavior of H adatoms on W surfaces can be considered as an independent subsequent pro-

cess and beyond the scope of the present paper.

4. Discussion and conclusions

We performed MD simulations to study the diffusion behavior of H isotopes in single-crystal W. Several concepts were clarified by the MD simulation results. First, in the considered temperature range, the slight non-Arrhenius behavior of the diffusion coefficient of H isotopes in W indeed exists. Second, many-body effects reduce the sensitivity of the dependence of the pre-factor of the diffusion coefficient on the isotope mass, although the anharmonic effect of the potential surface induces a very slight dependence of the activation energy on isotope mass. Third, no trap mutations occur for H atoms diffusing near either the W{100} or W{111} surfaces, in contrast to the analogous cases for He atoms.

These conclusions were obtained for dilute interstitial H atoms in single W crystals. According to previous DFT and MD results,[19,42] H–H interactions at short distances in the W lattice are repulsive. The diffusion path of an interstitial H atom can be obstructed by neighboring H atoms. Based on this picture, a kinetic Monte Carlo (KMC) method was used by Yang *et al.*[43] to study the concentration dependence of the diffusion coefficient of H in single-crystal W. The concentration effects on D diffusion in W have also been studied by Ahlgren and Bukonte[44] based on MD simulations. They showed that the diffusion coefficient deviated significantly from the low concentration limit when the D/W ratio was above 0.01. We have also conducted MD simulations with various H/W ratios in the simulation boxes, arriving at a conclusion similar to that of Ahlgren and Bukonte. To assess the applicability of the diffusion coefficient obtained in the case of dilute interstitial H isotopes in single-crystal W, we calculated the time evolution of the concentration distribution of interstitial H atoms in a semi-infinite W substrate irradiated by energetic H projectiles. Assuming the concentration distribution at time t is $n(z,t)$, based on the model established in subsection 3.3, the concentration distribution at time $t+\Delta t$ can be expressed

$$n(z,t+\Delta t) = \int_0^{\infty} \frac{1}{2(\pi D\Delta t)^{\frac{1}{2}}} \left[\exp\left(\frac{-(z-z_0)^2}{4D\Delta t} \right) - R\cdot \exp\left(\frac{-(z+z_0)^2}{4D\Delta t} \right) \right] \times [n(z_0,t)+s(z_0,t)]\,\mathrm{d}z_0, \quad (8)$$

where $s(z,t)$ is the depth distribution of the H source. If the incident flux of H projectiles is Γ, $s(z,t)$ is written

$$s(z,t) = \Gamma\Delta t\,(1-R_{\mathrm{f}})\,f(z), \quad (9)$$

where R_{f} is the reflection coefficient and $f(z)$ is the range distribution of the H projectiles. We calculated R_{f} and $f(z)$ using the bipartition method for solving the Boltzmann transport equation of projectiles in materials.[45] Moreover, the setup of the time step Δt and the size of the depth grid $\mathrm{d}z_0$ can be justified by checking the conservation of particle number.

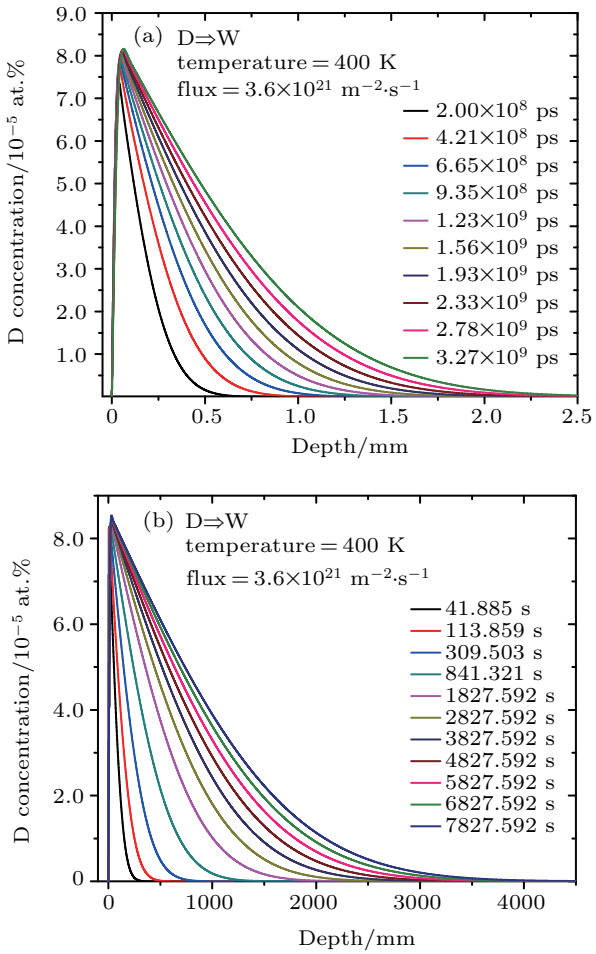


Fig. 6. (color online) Time evolution of the concentration distribution of D implanted in perfect W at 400 K. The incident flux of D is 3.6×10^{21} m^{-2}·s^{-1}: (a) 0.0002–0.00327 s, (b) 41.885–7827.592 s.

As an example, we considered 200 eV D projectiles irradiated on W at 400 K with $\Gamma = 3.6\times10^{21}$ m^{-2}·s^{-1}. The reflection coefficient is 0.606. Figure 6 shows the evolution of the concentration distribution in the D/W ratio. As time elapses, the concentration distribution spreads out in depth. The maximum concentration, near a depth of 0.1 μm, increases initially and then tends to maintain a D/W ratio of 8.5×10^{-7}. This value is lower than 0.01 by four orders of magnitude. If we adopt $\Gamma = 3.6\times10^{24}$ m^{-2}·s^{-1}, which is within an order of magnitude of the highest flux reported in the experimental literature, the maximum concentration would be 8.5×10^{-4}. We also calculated the retention of D atoms, which is defined by $\bar{n}(t) = \int_0^{\infty} n(z,t)\,\mathrm{d}z$. Figure 7 illustrates $\bar{n}(t)$ (m^{-2}) versus time t (s) for $\Gamma = 3.6\times10^{21}$ m^{-2}·s^{-1}, in which $\bar{n}(t)$ is proportional to the square root of t and can be well fitted by the equation $\bar{n}(t) = 6.607\times10^{17}\times t^{0.5}$. The observation that D retention is proportional to the square root of time was also observed in Refs. [16] and [46] . At the fluence $\Phi = 3.60\times10^{24}$ m^{-2} ($t = 1000$ s), $\bar{n}(t)$ is $\sim 2.09\times10^{19}$ m^{-2}.

This suggests that most of the implanted D atoms have escaped from the substrate. One reason for this is the shallow range distribution. The range over which 200 eV D projectiles continuously slow is ~ 0.016 μm.

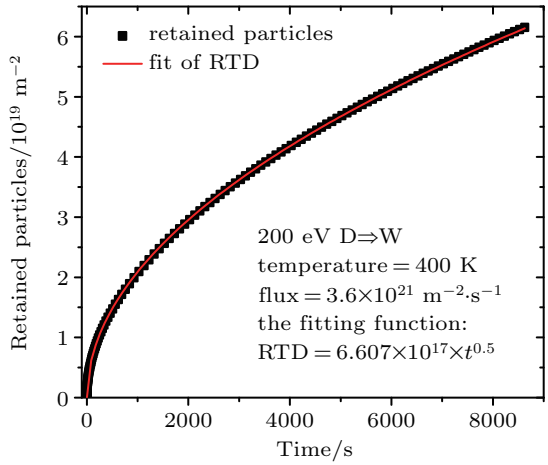


Fig. 7. (color online) Retention of D as a function of time. The D atoms are implanted in perfect W at 400 K with an incident flux of 3.6×10^{21} m^{-2}·s^{-1}.

From the calculation results, the concentration of interstitial D atoms in single-crystal W irradiated by low-energy H isotopes is clearly much lower than that when the concentration effects of interstitial D atoms on diffusion must be considered. Additionally, we should note that the influence of defects, such as vacancies and grain boundaries which usually exist in experimental samples and form trapping sites for H isotopes, on the diffusion of H isotopes was not considered in the foregoing calculations. Trapping sites may block the diffusion of H isotopes and build up their concentration in the shallow region of the substrate. However, the immobile, trapped H isotopes would contribute the principal portion of the concentration. The concentration of interstitial H isotopes should be reduced by the presence of trapping sites. Thus, unless the concentration of trapping sites is high, the diffusion coefficient obtained for dilute interstitial H isotopes should be applicable to, for example, rate-equation-based modelling in which trapping of H isotopes is included.

References

[1] Rieth M, Dudarev S L, Gonzalez de Vicente S M, *et al.* 2013 *J. Nucl. Mater.* **432** 482
[2] Ueda Y, Lee H T, Ohno N, Kajita S, Kimura A, Kasada R, Nagasaka T, Hatano Y, Hasegawa A, Kurishita H and Oya Y 2011 *Phys. Scr.* **T145** 014029
[3] Linsmeier Ch, Rieth M, Aktaa J, *et al.* 2017 *Nucl. Fusion* **57** 092007
[4] Taylor N, Merrill B, Cadwallader L, Di Pace L, El-Guebaly L, Humrickhouse P, Panayotov D, Pinna T, Porfiri M-T, Reyes S, Shimada M and Willms S 2017 *Nucl. Fusion* **57** 092003
[5] Tanabe T 2014 *Phys. Scr.* **T159** 014044
[6] Roth J and Schmid K 2011 *Phys. Scr.* **T145** 014031
[7] Causey R A and Venhaus T J 2001 *Phys. Scr.* **T94** 9
[8] Ueda Y, Schmid K, Balden M, Coenen J W, Loewenhoff T, Ito A, Hasegawa A, Hardie C, Porton M and Gilbert M 2017 *Nucl. Fusion* **57** 092006
[9] Watanabe T, Kaneko T, Matsunami N, Ohno N, Kajita S and Kuwabara T 2015 *J. Nucl. Mater.* **463** 1049
[10] Roszell J P, Davis J W and Haasz A A 2012 *J. Nucl. Mater.* **429** 48
[11] García-Rosales C, Franzen P, Plank H, Roth J and Gauthier E 1996 *J. Nucl. Mater.* **233** 803
[12] Frauenfelder R. 1969 *J. Vac. Sci. Technol.* **6** 388
[13] Franzen P, Garcia-Rosales C, Plank H and Alimov V K 1997 *J. Nucl. Mater.* **241** 1082
[14] Guterl J, Smirnov R D, Krasheninnikov S I, Zibrov M and Pisarev A A 2015 *Nucl. Fusion* **55** 093017
[15] Poon M, Haasz A A and Davis J W 2008 *J. Nucl. Mater.* **374** 390
[16] Ogorodnikova O V. 2009 *J. Nucl. Mater.* **390** 651
[17] Gasparyan Y M, Ogorodnikova O V., Efimov V S, Mednikov A, Marenkov E D, Pisarev A A, Markelj S and Čadež I 2015 *J. Nucl. Mater.* **463** 1013
[18] Lu G H, Zhou H B and Becquart C S 2014 *Nucl. Fusion* **54** 86001
[19] Liu Y L, Zhang Y, Luo G N and Lu G H 2009 *J. Nucl. Mater.* **390** 1032
[20] Xu J and Zhao J 2009 *Nucl. Instrum. Methods Phys. Res. B* **267** 3170
[21] Johnson D F and Carter E A 2010 *J. Mater. Res.* **25** 315
[22] Heinola K and Ahlgren T 2010 *J. Appl. Phys.* **107** 113531
[23] Fernandez N, Ferro Y and Kato D 2015 *Acta Mater.* **94** 307
[24] Picraux S T and Vook F L 1974 *Phys. Rev. Lett.* **33** 1216
[25] Wang J, Zhou Y, Li M and Hou Q 2012 *J. Nucl. Mater.* **427** 290
[26] Wen H, Semenov A A and Woo C H 2017 *J. Nucl. Mater.* **493** 21
[27] Perez D, Vogel T and Uberuaga B P 2014 *Phys. Rev. B* **90** 014102
[28] Hammond K D and Wirth B D 2014 *J. Appl. Phys.* **116** 143301
[29] Hu L, Hammond K D, Wirth B D and Maroudas D 2014 *Surf. Sci.* **626** 21
[30] Wang X, Wu Z and Hou Q 2015 *J. Nucl. Mater.* **465** 455
[31] Hou Q, Li M, Zhou Y, Cui J, Cui Z, Wang J 2013 *Comput. Phys. Commun.* **184** 2091
[32] Bonny G, Grigorev P and Terentyev D 2014 *J. Phys.: Condens. Matter* **26** 485001
[33] Marinica M C, Ventelon L, Gilbert M R, Proville L, Dudarev S L, Marian J, Bencteux G and Willaime F 2013 *J. Phys.: Condens. Matter* **25** 395502
[34] Henkelman G and Jónsson H 2000 *J. Chem. Phys.* **113** 9978
[35] Henkelman G, Uberuaga B P and Jónsson H 2000 *J. Chem. Phys.* **113** 9901
[36] Shu X, Tao P, Li X and Yu Y 2013 *Nucl. Instrum. Methods Phys. Res. B* **303** 84
[37] Wen H, Semenov A A and Woo C H 2017 *J. Nucl. Mater.* **493** 21
[38] Boisvert G and Lewis L 1996 *Phys. Rev. B* **54** 2880
[39] Liu Y N, Wu T, Yu Y, Li X C, Shu X and Lu G H 2014 *J. Nucl. Mater.* **455** 676
[40] Vineyard G H 1957 *J. Chem. Phys. Solids* **3** 121
[41] Hodille E A, Založnik A, Markelj S, Schwarz-Selinger T, Becquart C S, Bisson R and Grisolia C 2017 *Nucl. Fusion* **57** 056002
[42] Henriksson K O E, Nordlund K, Krasheninnikov A and Keinonen J 2005 *Appl. Phys. Lett.* **87** 163113
[43] Yang X and Oyeniyi W O 2017 *Fusion Eng. Des.* **114** 113
[44] Ahlgren T and Bukonte L 2016 *J. Nucl. Mater.* **479** 195
[45] Hou Q, Luo Z and An Z 1994 *J. Appl. Phys.* **76** 5690
[46] Bauer J, Schwarz-Selinger T, Schmid K, Balden M, Manhard A and Von Toussaint U 2017 *Nucl. Fusion* **57** 086015